Biological Logic Gate Using Gold Nanoparticles and Fluorescence Lifetime Imaging Microscopy

Eran A. Barnoy,[†] Menachem Motiei,[†] Chen Tzror,[†] Shai Rahimipour,[‡] Rachela Popovtzer,[†] and Dror Fixler*[,†]

[†]Faculty of Engineering and the Institute of Nanotechnology and Advanced Materials, Bar Ilan University, Ramat Gan 5290002, Israel

[‡]Department of Chemistry, Bar Ilan University, Ramat Gan 5290002, Israel

ABSTRACT: Current medicine could greatly improve by intelligent treatment systems able to respond autonomously to early stages of diseases from within a patient. As an initial study en route to such a system, we describe biologically relevant logic gates based on gold nanoparticles (GNPs) and fluorescent molecules that are able to respond to multiple input parameters so as to detect specific biological conditions all through the lens of fluorescence lifetime (FLT) imaging microscopy (FLIM). By conjugating the pH-responsive Oregon Green 488 (OG) to the GNPs by a trypsin-cleavable peptide, we manufactured GNP−OG constructs, which are responsive to two separate inputs: surrounding pH and proteinase presence. The GNP−OG constructs can sensitively detect and distinguish between conditions of low pH and no enzyme, the presence of one of either raised pH or enzyme, and the presence of both. Additionally, the GNP−OG probes were tested on ex vivo mouse organs to demonstrate further biological relevance and successfully behaved as various logic gates would be expected in different organs where pH and enzyme conditions vary. Altogether, the GNP−OG constructs are shown to carry out logic gate behaviors, where the desired gate is defined by the FLT detected. Unlike previous biological logic gates, the GNP−OG constructs can realize AND, OR, NAND, NOR, XOR, and XNOR gates by choosing different FLT cutoffs alone. The constructs make for efficient fluorescent logic detectors independent of concentration and so can serve as a stepping stone toward more complex logic systems.

KEYWORDS: gold nanoparticles, biological logic gate, chemical imaging, bioresponsive, bioswitch, fluorescence lifetime imaging
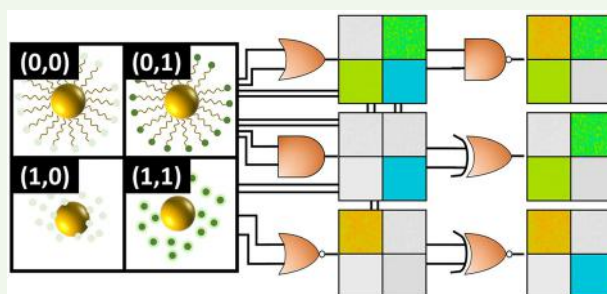
INTRODUCTION

Modern medicine could be greatly improved by smart, patient-specific therapies, able to act completely autonomously. Smart therapies would be able to bypass many issues such as the side effects resulting from systemic medication administration when only a specific part of the body requires attention.[1] Patient specificity would make therapies relevant to the patients who do not respond according to the statistically determined outcomes.[2] Finally, problems can arise from patient−doctor miscommunication, and a treatment able to administer itself in the correct time and place at appropriate dosages could significantly improve current standards.[3] To achieve all of these goals concurrently, these factors would seem to require a personal computer living within our bodies. However, the same effects can be established using a circulating network of responsive nanoparticles (NPs).

Gold NPs (GNPs) show much promise as intelligent theranostic agents for a variety of reasons. GNPs are relevant for all kinds of applications in medicine, engineering, and chemistry[4] due to the ease with which they can be functionalized,[5,6] their nontoxicity and biocompatibility,[7] and various optical properties, which include a large absorption cross-section[8] and tunable scattering characteristics.[9] The

combination of these factors grant GNPs the ability to significantly affect fluorophores in their vicinity, leading to substantial quenched or even metal-enhanced fluorescence (MEF).[10] GNP-aided techniques have already been developed for X-ray, computed tomography (CT), diffusion reflection (DR), surface-enhanced Raman scattering, and photoacoustic tomography, including phantom and in vivo experiments.[11−15] Our laboratory has previously shown many such capabilities of GNPs,[14,16,17] including the use of the enhanced permeation and retention effect to make systemic administration localized[18,19] and GNPs' enhancement of conjugated fluorophores and applicability as fluorescent probes in biological settings.[20−22] By combining these parameters, it can be straightforward to use GNPs as building blocks for potential nanorobots circulating in vivo.

When it comes to fluorescent imaging, fluorescence lifetime (FLT) imaging microscopy (FLIM) provides many benefits over conventional fluorescence intensity (FI) imaging. Besides inherently gathering FI information, FLIM also measures the

Scheme 1. Dual Biologically Relevant Stimuli: Enzyme Activity and Environmental Acidity[a]

Coating of 20 nm GNPs with fluorescent peptide

Neutral to high pH results in activated fluorophore

Peptide cleavage severs the connection of fluorophore to GNP

Presence of both higher pH and cleaving peptide results in longest FLT
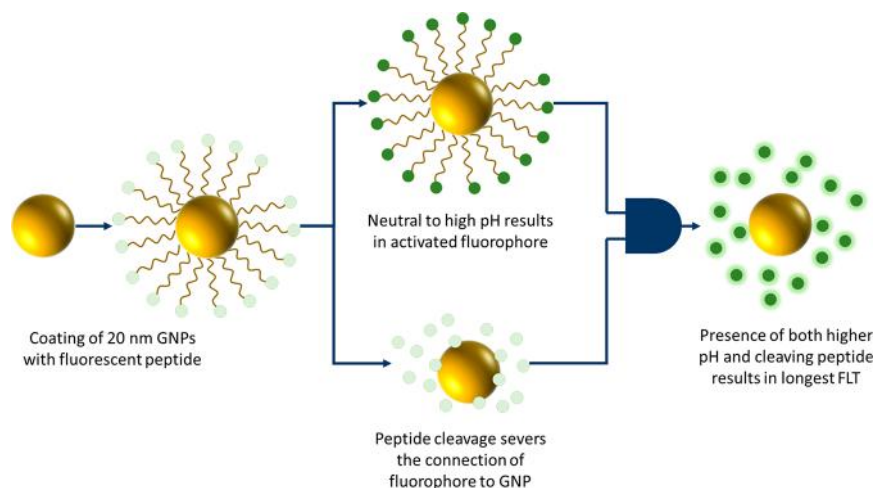
[a]Gold nanoparticles of 20 nm were coated with a reactive, fluorescent peptide. The fluorophore was chosen to respond to environmental pH, while the peptide was designed to be cleaved by certain enzymes. The presence of either trigger leads to partial activation, while the presence of both leads to full activation with the strongest fluorescent signal.

FLT of imaged samples, thus generating quantitative data useful for many biological and biomedical applications more reliably.[23−25] Traditional FI measures the intensity of the fluorescence signal of a sample but can only be interpreted qualitatively with limited quantitative comparability due to the sensitivity of the FI to such biologically fickle parameters as fluorophore concentration or excitation behavior. The FLT, however, is a known quantity for any fluorescent substance and is independent of molecule concentration or excitation intensity. Variations recorded by FLIM allow for intuitive quantitative analysis by detecting different biological environments or processes.[23,24] Within 40 nm from the surface of GNPs, fluorophores' FLT can vary due to the near-field interactions of the fluorophore and the GNP.[10,26−28] A change in proximity to GNPs can be deduced more accurately from FLT measurements than FI, making GNP−fluorophore constructs useful FLIM probes, and especially where the particle−fluorophore distance can be controlled on the basis of the environment. By following changes in FLT across an organism, FLIM could effectively use reactive fluorescent NPs to detect important biological processes in vivo.

Intelligent, or stimulus-activated NPs have been researched over the past 2 decades in order to improve the current quality of medications.[29] Several studies demonstrated engineered constructs that respond to multiple stimuli in a manner similar to computer logic gates, exhibiting behaviors of AND, OR, NAND, XOR, and others, so as to achieve intelligent abilities.[3,30−37] These smart NP systems also include variations of GNP-based probes.[38−40] Fluorescent GNP probes have usually been based on the removal of quenching, where GNP proximity reduces the FI and subsequent interaction (i.e., linker cleavage in the vicinity of specific enzymes) restores normal fluorescence.[41−44] Several other studies made use of MEF to provide greater contrast changes for activated states.[45−47] Although several such studies included FLT measurements, FLT was never the deciding factor able to differentiate the different logic situations but was rather dismissed due to its inflexibility under the static quenching situations used in their studies.[48−52]

In the ideal situation, multiple logical systems would interact with each other and, by their interaction, display behavior fitting to the very complex environments found within the human body and throughout the myriad diseases we face.[53] We are not at the age of nanocomputers functioning fully within our bodies, however, and there are many roadblocks on the way. As one of the possible avenues in this direction, our laboratory is developing optically observable nanologic constructs. We are able to visualize the functioning of these constructs, with the hope that they will allow detection by other nanoconstructs instead in the future and so lead to an intelligent yet autonomous chain of action.[54,55] In order to achieve this goal, we describe in this work, for the first time, a biologically stimulated system consisting of GNP and activatable fluorescence detectable by FLIM.

By combining GNPs and the FLIM imaging modality, we describe an optically discernible system able to respond to biologically relevant environments and signals in a behavior similar to computer logic gates. The constructs described here consist of a peptide linker between GNP and fluorophores, which was designed to be cleaved by the enzyme trypsin. Trypsin is a protease produced in proenzyme form in the pancreas and is subsequently activated and used for digestion in the small intestine.[56] The fluorophore chosen for our constructs is Oregon Green 488-X (OG), which has a pK_a of 4.7 and therefore has affected fluorescence in lower pH environments, such as those found in certain organelles. Together, the GNP−fluorophore distance controlled by the peptide, and fluorescence further determined by pH, we have a system able to respond to two biologically relevant stimuli— enzyme activity and environmental acidity (see Scheme 1). We show that the entire biological logic activity can be determined purely by FLIM, making these constructs exceptionally promising prototype biological logic-driven imaging tools.

■ METHODS

Chemicals and Components. Solutions of different pH levels were prepared by titrating controlled amounts of NaOH at various concentrations into HCl starting at 0.01 M and with constant monitoring by digital pH probe. Stock solutions were created in this manner for pH 1, 2, 3, 4, 5, and 6.

Trypsin solution B, containing 0.25% trypsin in DPBS with no calcium or magnesium, was acquired from Biological Industries (BI). The solution also contained no phenol red so as to not interfere with fluorescent measurements.

Oregon Green 488-X, succinimidyl ester, 6-isomer (OG), and the custom peptide used in this study were purchased from Thermo Fisher Scientific. The peptide was designed with the following structure: CGGWRK, with PEG12 between the cysteine and first guanine, acetylated n-terminus, and the OG bound to the c-terminus.

Nanoparticle Fabrication and Coating. Gold nanospheres of 20 nm diameter were synthesized according to the method of Enüstün and Turkevich.[57] For this process, 62.1 μL of 50% HAuCl4 solution was mixed into 30 mL of distilled water and then boiled. Upon boiling, magnetic stirring was started and 606 μL of 10% sodium citrate solution was added. The solution was stirred with heat for 5 min. After cooling, the new GNPs were placed in ice. Meanwhile, 1 mg of the OG peptide was suspended in 500 μL of double deionized water (DDW) and added to the particles. Another 500 μL of DDW was added to the peptide vial to make sure all came out and then also added to the particles, which were placed under renewed stirring. The particles and peptides were allowed to mix for 2.5 h, allowing for the thiol groups in the cysteine of the peptide to adsorb to the particle surface. The amount of peptide was chosen to completely coat the entire surface of the theoretical maximum particle yield, with excess. After mixing, the new GNP−OG constructs were gathered through repeated centrifugation, including repeated washing by adding plenty of DDW after each centrifugation process and repeating.

Single Gate Measurements. In this study, the GNP−OG constructs were tested under two methods of activation, or gates: fluorophore activation by pH and peptide cleavage by trypsin. In order to measure the response of the constructs to pH, 20 μL of GNP−OG solution was mixed with 180 μL of pH stock solution of each pH as described above. For reversibility experiments, 20 μL of GNP−OG solution was first mixed with 180 μL of pH 1 stock solution, and then 1 M NaOH 1 μL at a time until the color of the solution visibly turned from purple to pink. For trypsin experiments, solutions were made with 20 μL of GNP−OG solution mixed with 100 μL of 0.25% trypsin solution B, raised to 200 μL with DDW, and then placed in an incubator at 37 °C for 1 h. For lowering the pH after trypsin cleavage, pH 1 stock solution was added 1 μL at a time until the color of the solution visibly turned from pink to purple.

Ex Vivo Imaging. For ex vivo experiments, a healthy 2 month old male BALB/c mouse was sacrificed, and the pancreas, small intestine, and stomach were excised. A slice of each organ was placed on Petri dishes. GNP−OG constructs were placed directly on the exposed inner section of each organ, and these Petri dishes were placed in an incubator at 37 °C with the exposed section—and GNPs—facing up. Meanwhile, other dishes containing organs with exposed inner sections facing down and without particles were taken to be imaged by FLIM. One hour after placement in the incubator, the organ slices exposed to the GNPs were flipped so that the exposed inner section faced downward, and these were also taken to the FLIM. All use of live animals was approved by the Bar Ilan University Institutional Animal Care and Use Committee and is in compliance with rules set by the National Institutes of Health according to the Guide for the Care and Use of Laboratory Animals, DHEW (NIH, Pub. 78-23).

FLIM Measurements: FI and FLT. The FLT measurements described in this work were carried out using an inverted two-channel laser scanning confocal microscope system (DCS 120, Becker & Hickl GmbH, Berlin, Germany). The full width at half-maximum (fwhm) of the excitation pulse is of the order of 10−100 ps. For these images, 256 × 256 pixel sample areas were excited by 20 MHz, 473 nm laser pulses and detected using a 495 nm LP filter and 1.0 mm pinhole. Each sample was measured at least 4 times for 180 s per measurement, and fluorescence was recorded using a time-correlated single photon counting (TCSPC) card.

Fluorescence analysis, exponential fitting, and FLIM image generation were carried out using the software SPCImage v. 5.3 (Becker & Hickle GmbH 2015, Berlin, Germany). Other statistical analyses and plots were created in the statistical package R v. 3.1.1 (R

Core Team 2014. R: A language and environment for statistical computing. R Foundation for Statistical Computing, Vienna, Austria).

Solutions only required a single exponential for good fitting (χ^2 values near unity), but organs were all fit to two exponentials. The FLT values described for the organ images are the amplitude weighted averages of the two components.

RESULTS

OG Characterization. Although the pK_a of OG is 4.7 and its FI has been explored as a function of pH,[58] we first sought to characterize the combined FI and FLT information we were able to obtain using FLIM according to the process described in Methods. All measurements were taken from free OG in a solution of the corresponding pH, with identical concentrations in each solution and identical imaging conditions. Figure 1 depicts both FLIM images as well as corresponding
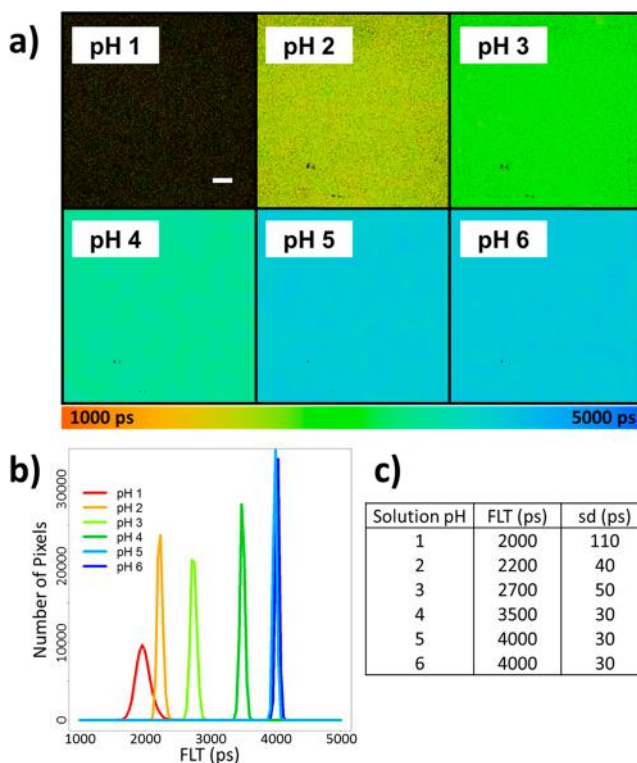
Figure 1. Oregon Green 488 (OG) fluorescence lifetime (FLT), in solutions of different pH: (a) FLIM images, (b) histograms of the FLT values found in the pixels of the images, and (c) corresponding means and standard deviations. All images are in the same scale for fluorescence intensity (FI). For all FLIM images, the scale bar is as shown in the top-left image and measures at 100 μm.

FLT histograms to display the increasing FLT in response to increasing pH from 1 to 6. It is apparent that while the FLT gradually increases with pH from values averaging around 2 ns at pH 1, the FLT for both pH 5 and 6 are essentially identical at about 4 ns. This same FLT of 4 ns was seen again at pH 7 and 10 (data not shown). This value matches reported OG FLT measurements.[59] For our purposes, we can identify the OG molecules as "fully activated" (the "1" state) at pH greater than 4 and as "not activated" or "partially activated" ("0" state) for lower pH values.

GNP−OG Characterization. GNPs of 20 nm were synthesized and subsequently coated with a peptide cleavable by the enzyme trypsin and containing OG molecules, as
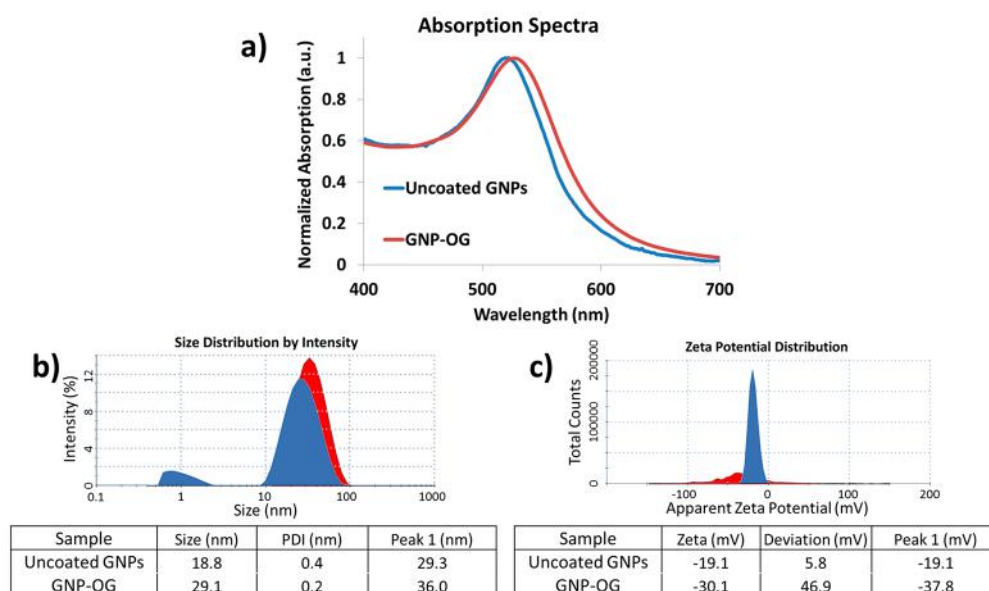
Figure 2. Gold nanoparticles (GNPs) before and after coating with peptide and OG: (a) absorption spectra, (b) DLS, and (c) ζ potential measurements. In all three images, uncoated GNPs are shown in blue and GNP−OG constructs in red.

described in Methods. These particles were characterized by absorption spectra, DLS, and ζ charge measurements before and after conjugation (see Figure 2). While the absorption peak of the uncoated particles was 520 nm, the GNP−OG constructs peak was at 527 nm and with a broadened distribution. DLS measurement main peaks changed from 29.3 nm when uncoated to 36.0 nm after coating. ζ potential averages decreased from −19.1 to −30.1 mV. All forms of characterization indicated successful coating of the GNPs.

GNP−OG pH Effects. The full GNP−OG construct, in theory, experiences FI quenching due to the GNP near-field effects, and subsequent trypsin cleavage should restore OG FI. However, as described above, OG exhibits pH-dependent behavior, so its behavior after conjugation to GNPs should also change with pH. In order to characterize these effects after binding, we measured the FI and FLT of the GNP−OG constructs in solutions of varying pH from 1 to 6, as well as in saline and PBS. All measurements were performed on solutions of identical GNP−OG concentrations with identical imaging conditions. The results of these measurements, including FLIM images and FLT distribution histograms, are displayed in Figure 3. As with the free dye in solution, the conjugated GNP−OG constructs respond to their surrounding pH accordingly, with low pH surroundings resulting in a FLT of about 1.8 ns, and more neutral or physiological surroundings having a FLT of approximately 3.1 ns. There still exists distinct pH-dependent responsiveness as with free OG, yet the FLT is significantly shorter with GNP than without.

Further marking the promise of this responsiveness is the constructs' ability to demonstrate this behavior in a reversible manner. Figure 4 shows GNP−OG solutions at very low pH (pH 1), followed by the FLIM images after raising a solution of GNP−OG in pH 1 to acidity levels that allow for the physiological FLT response. Even with FLT values dropping by initial acidity, the restoration of the environment also restored the longer FLT, as can be seen in the similarity between the condition of pH 1, raised, to a control GNP−OG solution in pH 6 (3.2 ± 0.1 ns vs 3.1 ± 0.1 ns, respectively).
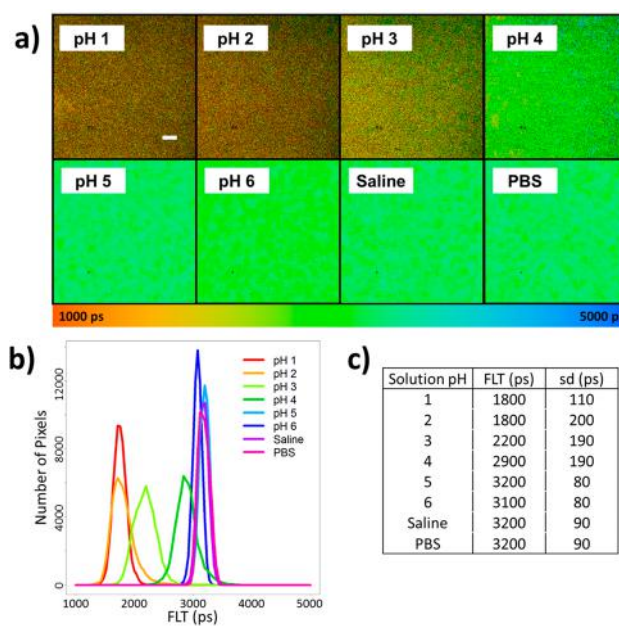
Figure 3. GNP−OG FLT response in different pH solutions: (a) FLIM images, (b) histograms of the FLT values found in the pixels of the images, and (c) corresponding means and standard deviations. All images are in the same scale for FI. For all FLIM images, the scale bar is as shown in the top-left image and measures at 100 μm.

GNP−OG Trypsin Effects. After determining the sensitivity of the GNP−OG constructs to one form of activation, we tested their ability to respond to another activation: peptide cleavage by trypsin. The peptide used to link the GNPs and OG, described in Methods, was designed to be cleavable by the enzyme trypsin. In order to test enzyme response, solutions of GNP−OG were incubated together with trypsin at 37 °C and subsequently imaged using FLIM. Figure 5 shows FLIM images, as well as FLT distribution histograms for GNPs incubated in water, GNPs incubated with trypsin, and GNPs incubated with trypsin and later having the pH
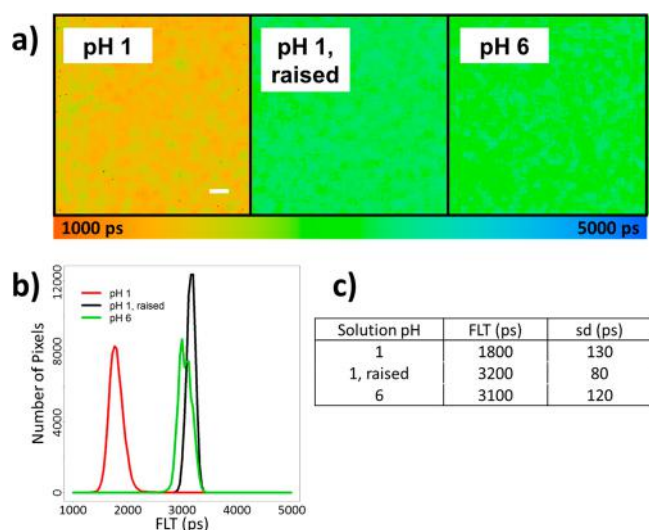
Figure 4. GNP–OG FLT response following lowered and subsequently raised pH: (a) FLIM images, (b) histograms of the FLT values found in the pixels of the images, and (c) corresponding means and standard deviations. A solution made of GNPs in pH 6 was also prepared as a control. There is no FI information here. For all FLIM images, the scale bar is as shown in the left image and measures at 100 μm.
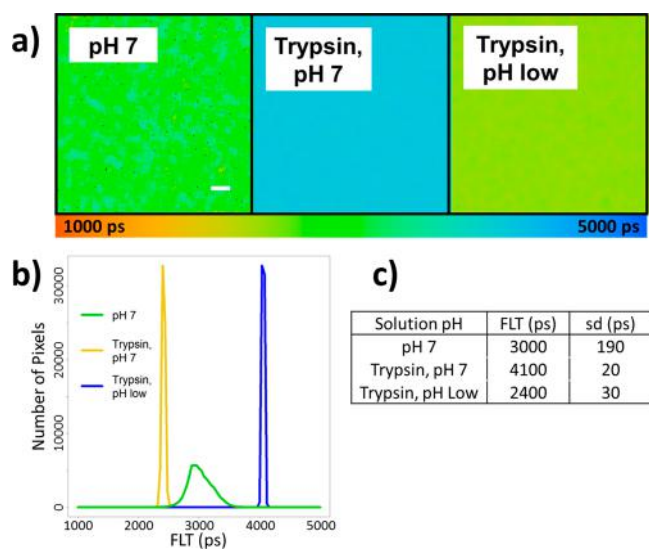
Figure 5. GNP–OG response to co-incubation with trypsin as well as a combination of trypsin and lowered pH: (a) FLIM images, (b) histograms of the FLT values found in the pixels of the images, and (c) corresponding means and standard deviations. For all FLIM images, the scale bar is as shown in the left image and measures at 100 μm.

lowered. While GNPs in water displayed results similar to those reported above (3.0 ± 0.2 ns), trypsin significantly raised the FLT to that of free OG in solution (4.0 ± 0.02 ns). When the constructs experience both trypsin activation and lowered pH, the FLT drops as with free OG (2.4 ± 0.03 ns). Here we see a second activation process able to affect the fluorescence characteristics of the constructs. Taken together, the response to both trypsin cleavage and pH marks the biological logic gate potential of these constructs.

Implementing GNP–OG Logic Gates of ex Vivo Organs. Finally, in order to demonstrate the biological

relevance of the GNP–OG constructs, they were placed on various mouse organs ex vivo. Trypsin is a naturally occurring enzyme, where its proenzyme is produced in the pancreas, and the enzyme is fully activated in the small intestine.[56] Both of these organs naturally contain physiological pH values— approximately neutral. Meanwhile, in its role in the digestion process, the stomach employs low pH and the enzyme pepsin (among others) to cleave peptides. Unlike trypsin, which only functions at physiological pH, pepsin requires low pH in order to function.[60] The peptide used in this study to connect GNPs and OG is susceptible to both pepsin and trypsin. As such, we checked our ability to see our constructs in mouse pancreas, small intestine, and stomach. Each of these provides different regions of interest: no trypsin and neutral pH (pancreas), trypsin and neutral pH (small intestine), and trypsin-like enzyme and low pH (stomach). FLIM images of these organs with and without GNPs are shown in Figure 6. The results reveal that although an autofluorescence is detected in the organs alone, a FI signal stronger by over an order of magnitude is found with GNPs. In terms of FLT, it is also evident that the presence of a cleaving enzyme and/or different pH values results in different FLIM results. We see the highest FLT values in the small intestine where we observe both cleavage and high pH (3.4 ± 0.2 ns), an intermediate FLT in the pancreas with high pH but no cleavage (3.0 ± 0.1 ns), and the lowest FLT in the stomach with cleavage but low pH (1.6 ± 0.3 ns). The previous results indicated that the GNP–OG constructs respond to an arbitrary amount of trypsin in solution, and here we have shown that also the amounts of these enzymes found in organs trigger measurable responses. The organ-specific behaviors indicate that these simple GNP–OG constructs are able to respond to different biologically relevant situations accordingly, and differently from autofluorescence.

◼ DISCUSSION

Considering the results represented in Figure 5 and Figure 6, it easily follows that the GNP–OG constructs can be defined to follow different logic operations based on the FLT. First, we would define the "inputs" to our system as pH and enzyme. By defining a situation of low pH and no enzyme as (0,0), one with no enzyme and neutral pH as (0,1), one with enzyme and low pH as (1,0), and both enzyme and neutral pH as (1,1), we can reorganize the results to clearly mark the different logic operations possible in this system (see Figure 7a). Then, it is possible to assign different logic gate behaviors to any result simply by choosing the correct cutoff in FLT for defining the "output" (Figure 7b). Different logic gates determine when an output is defined as achieved —1—or not—0—based on the presence or absence of the inputs. For our two-input logic gates, an OR gate provides an output of 1 if at least one of the inputs is present. An AND gate has output 1 only when both inputs are present. A NOR gate has output 1 when neither of the inputs is present—the opposite of an OR. Similarly, a NAND gate has output 1 in all situations except when both inputs are present. A XOR gate has output 1 when exactly one of the inputs is present, and a XNOR gate has output 1 either when neither input is present or when both are together. For the current system, only the situations with the highest FLT (above 3.5 ns) mark an AND situation where both inputs are present, we can lower the cutoff (above 2.0 ns) to define OR situations, flip these cutoffs to define NOR (below 2.0 ns) and NAND (below 3.5 ns), only consider medium FLT values for a
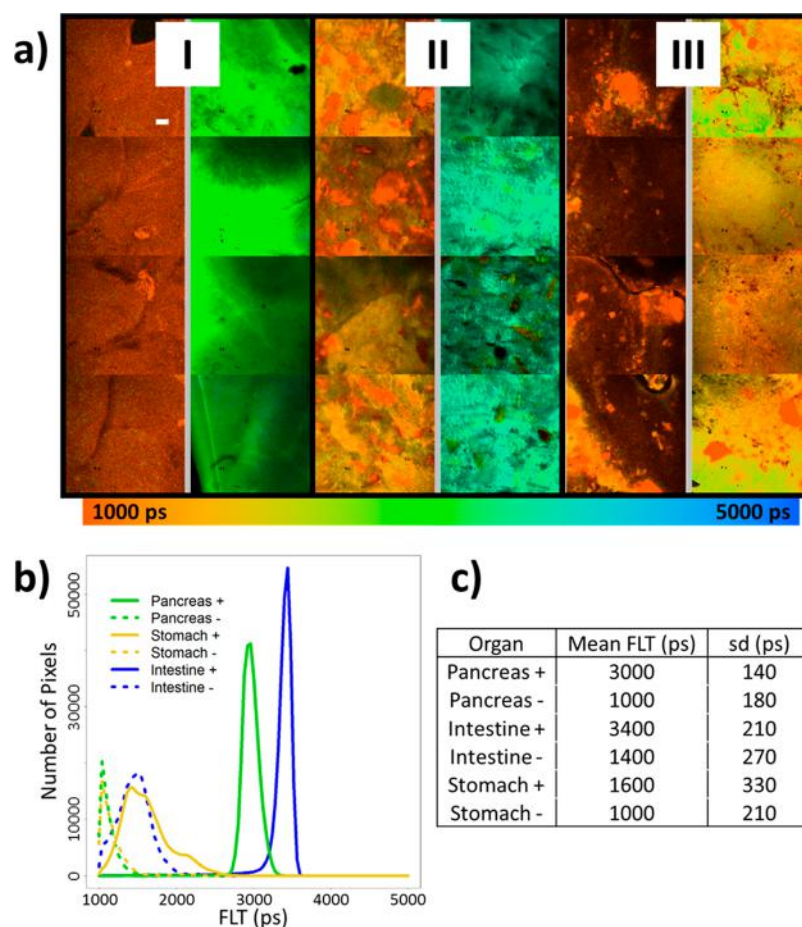
Figure 6. GNP−OG FLT response to different mouse organs ex vivo: (a) FLIM images, (b) histograms of the FLT values found in the pixels of the images, and (c) corresponding means and standard deviations, where "+" indicates with GNPs and "−" indicates without. The organs shown are (I) pancreas, (II) small intestine, and (III) stomach, where the organs without GNP−OG are shown on the left and with on the right. For all FLIM images, the scale bar is as shown in the top-left image and measures at 100 μm.

XOR gate (above 2.0 ns and below 3.5 ns), and consider the highest and lowest values for a XNOR gate (below 2.0 ns or above 3.5 ns). Both from behaviors in solutions and from those in ex vivo organs, the GNP−OG constructs display clear biological logic gate capabilities.

The value of using FLIM for logic gate definitions is precisely this ability to select cutoff values. Whereas logic gates based on FI may detect low, high, and intermediate distinct signals, the FLT values are much more reproducible, and do not depend on excitation or detection parameters or nanoparticle concentration. The same cutoff values, such as the 3.5 and 2.0 ns mentioned above, could be used whenever the measurement is repeated. With the repeatability and quantifiability of FLIM in mind, the desired cutoff and gate would need to be determined before measurements and screening. Scientists or caregivers would need to determine in advance whether the condition being studied would be relevant in an AND, OR, NAND, NOR, XOR, or XNOR situation. Thus, for example, if it is enough to determine a disease based only on the presence of one of the inputs, then we would consider only an OR gate and determine that a positive output is when the FLT is 2.0 ns or longer. Meanwhile, if the disease can only be determined by having both inputs present together, then an AND gate would be considered, and a positive output would be defined as the situation when the FLT is longer than 3.5 ns.

While the success of this simple classification is heartening, it is worthwhile to explore some important issues that were raised by the experiments. First, trypsin requires a neutral pH in order to function properly, thereby not allowing for simultaneous "input" of trypsin and low pH. In this manner, trypsin and solution pH are not truly orthogonal conditions. When considering only trypsin, the theoretical (1,0) situation is biologically impossible, at least simultaneously. For this reason, the results in Figure 5 had to simulate a simultaneous (1,0) situation by only lowering the pH after trypsin activation. However, by looking at the broader viewpoint of the two inputs considered in this system as "enzyme cleavage" and "solution pH", this condition becomes possible. This viewpoint is exemplified by the ex vivo results, where, owing to the fact that multiple enzymes are able to cleave the GNP−OG peptide, pepsin also served to cleave the peptide but at low pH, thereby achieving a true (1,0) state.

The sensitivity to multiple enzymes provides two possible avenues of applicability to the probes discussed here. First, the ability to detect both pepsin and surrounding pH could have meaningful applications such as in damaging reflux situations, where detecting pepsin together with nearby acidity can help reveal reflux situations and related airway diseases.[61] A smart probe could be especially useful since pepsin can linger in the esophagus, remain stable up to neutral pH, and then regain its activity when the pH drops again, leading to possible
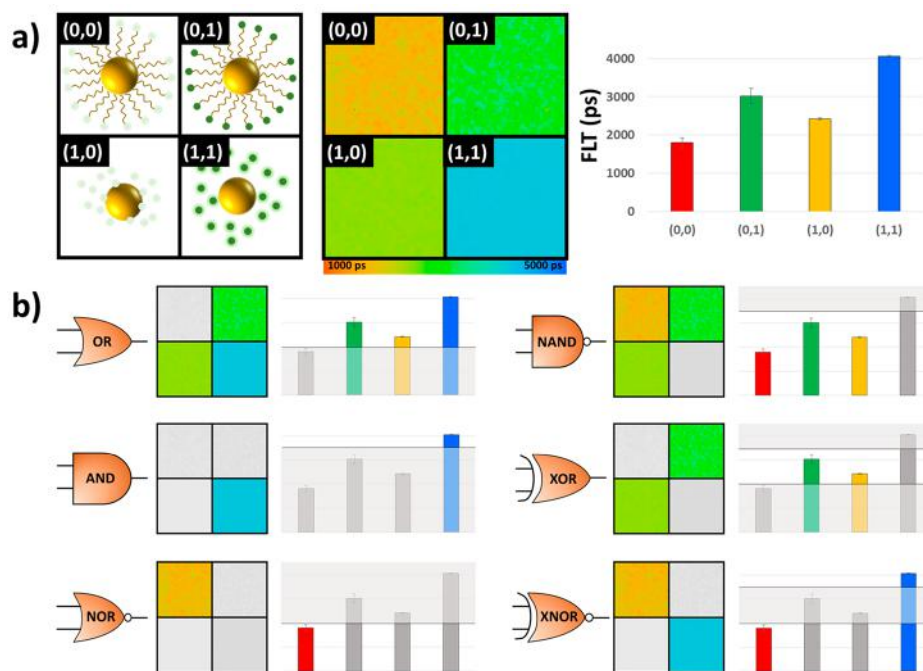
Figure 7. GNP−OG constructs displaying logic gate behavior by their FLT. (a) Previous results have been reorganized into the logic conditions outlined by Scheme 1 and detected by FLIM, as well as displayed by bar graph. (b) By choosing different cutoffs for the FLT, it is possible to define different logic operations. The different operations are shown here using the same FLIM image panels and bar graphs as before, except that the panels or bars corresponding to values outside the cutoffs have been grayed out.

esophegial damage.[62] GNP−OG used as a XOR gate could reveal potentially dangerous but latent pepsin and used as an AND gate would reveal the dangerous situations in real time. Second, the probes discussed can serve as a template for other applications that might be more appealing. It would be a simple matter to replace the enzyme-sensitive peptide in our system with a peptide susceptible to a different enzyme, and the fluorophore to another sensitive fluorophore—a change in the detectable inputs. For example, several cancers display heightened levels of matrix metalloproteinase activity in addition to the acidity found in tumor environments.[63,64] With simple modifications to the GNP−OG, we could construct FLIM-detectable smart cancer probes that would provide a long FLT only when there is both MMP-2 AND tumor acidity.

The issue of reversibility of the imaging probe is also important for discussion. While a cascade in events, where different constructs activate others in sequential fashions, is interesting and can be extremely useful in identifying and even treating biological conditions, there are major drawbacks inherent in an irreversible scheme that does not allow for complex logic responses. In irreversible situations, such as when a fluorophore is permanently cut off from the near-field effects of the GNPs, there is no way to recognize or respond if conditions change again. The constructs have one shot, and after an effect such as peptide cleavage, further studies would require the insertion of brand new constructs. On the other hand, a reversible response such as that of the GNP−OG to pH here is favorable. Logic operators working solely on reversible notions would be able to circulate for an extended time in a body and reveal changing conditions in either positive or negative directions.

CONCLUSIONS AND FUTURE DIRECTIONS

Through this work, we are advocating the development of smarter biological probes, to which this work serves as one of the stepping stones on the way to better medical diagnostics. There is still a lot of work to be done in the field, and as discussed, the GNP−OG constructs are not perfect. However, they do serve to display probes that (1) are activated by multiple possible biologically relevant conditions, (2) have been shown to activate as expected in actual biological tissue, and (3) have their behavior in biological settings efficiently described by the quantitative yet simple tool of FLIM. The ability to detect logic operations using our construct is demonstrated in Figure 7. As can be seen, by selecting different parameters for the FLT, it is possible to define different logic gates from FLIM results of our constructs. Logic gates based on FI cannot predefine the logic operations they attempt to detect because FI results depend on both excitation and detection parameters and so are inherently not as repeatable and quantifiable as FLT results. FLIM as a measurement device offers this opportunity to predefine the values in which we are interested and so presents a powerful biological logic gate analysis tool.

Although successful, there are necessary improvements raised as a response to our work. First, the constructs would need to advance to in vivo situations. While the promising results of the ex vivo measurements are encouraging, there is still no substitute for real situations in living organisms. Second, there is the option of optimizing these constructs. For example, by using gold nanorods (GNRs), it is possible to reach surface plasmon peaks in the infrared spectrum—a set of wavelengths allowing for greater penetration through tissue.[22,65] It would then be possible to combine these particles of different surface plasmons with infrared fluorophores, and then achieve responses that allow for metal-enhanced effects

and so make them even better suited for fluorescent studies.[66] Third, as discussed previously, completely reversible systems would be best for creating reusable smart nanoparticulate devices. To achieve such functionality, we would need to replace the enzyme cleavage with some other kind of smart behavior. Possibly, instead of using proteinases, we could make use of enzymes to simply change the conformation of a peptide so as to affect GNP−OG separation but in a reversible manner.[31,67,68] Finally, it would be ideal to add a broader view to these particles by adding the ability to interact with other kinds of particles and even make networks where various constructs susceptible also to other inputs can affect each other in cascades.[69,70] The ability to have one kind of smart nanoparticle construct influence the behavior of the next would bring us closer to achieving computer-like logic systems.

■ AUTHOR INFORMATION

Corresponding Author
*E-mail: Dror.Fixler@biu.ac.il.

ORCID 🔟
Dror Fixler: 0000-0003-0963-7908

Notes
The authors declare no competing financial interest.

■ ACKNOWLEDGMENTS

■ REFERENCES

(1) Rosenblum, D.; Joshi, N.; Tao, W.; Karp, J. M.; Peer, D. Progress and Challenges towards Targeted Delivery of Cancer Therapeutics. *Nat. Commun.* **2018**, *9* (1), 1410.

(2) Meir, R.; Shamalov, K.; Sadan, T.; Motiei, M.; Yaari, G.; Cohen, C. J.; Popovtzer, R. Fast Image-Guided Stratification Using Anti-Programmed Death Ligand 1 Gold Nanoparticles for Cancer Immunotherapy. *ACS Nano* **2017**, *11* (11), 11127−11134.

(3) Sokolov, I. L.; Cherkasov, V. R.; Tregubov, A. A.; Buiucli, S. R.; Nikitin, M. P. Smart Materials on the Way to Theranostic Nanorobots: Molecular Machines and Nanomotors, Advanced Biosensors, and Intelligent Vehicles for Drug Delivery. *Biochim. Biophys. Acta, Gen. Subj.* **2017**, *1861* (6), 1530−1544.

(4) Nie, S.; Xing, Y.; Kim, G. J.; Simons, J. W. Nanotechnology Applications in Cancer. *Annu. Rev. Biomed. Eng.* **2007**, *9*, 257−288.

(5) Blanco, E.; Shen, H.; Ferrari, M. Principles of Nanoparticle Design for Overcoming Biological Barriers to Drug Delivery. *Nat. Biotechnol.* **2015**, *33* (9), 941−951.

(6) Haimov, E.; Weitman, H.; Polani, S.; Schori, H.; Zitoun, D.; Shefi, O. Meso-Tetrahydroxyphenylchlorin-Conjugated Gold Nanoparticles as a Tool To Improve Photodynamic Therapy. *ACS Appl. Mater. Interfaces* **2018**, *10* (3), 2319−2327.

(7) Eghtedari, M.; Liopo, A. V.; Copland, J. A.; Oraevsky, A. A.; Motamedi, M. Engineering of Hetero-Functional Gold Nanorods for the in Vivo Molecular Targeting of Breast Cancer Cells. *Nano Lett.* **2009**, *9*, 287−291.

(8) El-Sayed, M. A. Some Interesting Properties of Metals Confined in Time and Nanometer Space of Different Shapes. *Acc. Chem. Res.* **2001**, *34* (4), 257−264.

(9) Jain, P. K.; Lee, K. S.; El-Sayed, I. H.; El-Sayed, M. A. Calculated Absorption and Scattering Properties of Gold Nanoparticles of Different Size, Shape, and Composition: Applications in Biological Imaging and Biomedicine. *J. Phys. Chem. B* **2006**, *110* (14), 7238−7248.

(10) Lakowicz, J. R. Radiative Decay Engineering 5: Metal-Enhanced Fluorescence and Plasmon Emission. *Anal. Biochem.* **2005**, *337* (2), 171−194.

(11) Copland, J. A.; Eghtedari, M.; Popov, V. L.; Kotov, N.; Mamedova, N.; Motamedi, M.; Oraevsky, A. A. Bioconjugated Gold Nanoparticles as a Molecular Based Contrast Agent: Implications for Imaging of Deep Tumors Using Optoacoustic Tomography. *Mol. Imaging Biol.* **2004**, *6* (5), 341−349.

(12) Qian, X.; Peng, X.-H.; Ansari, D. O.; Yin-Goen, Q.; Chen, G. Z.; Shin, D. M.; Yang, L.; Young, A. N.; Wang, M. D.; Nie, S. In Vivo Tumor Targeting and Spectroscopic Detection with Surface-Enhanced Raman Nanoparticle Tags. *Nat. Biotechnol.* **2008**, *26* (1), 83−90.

(13) Robinson, J. T.; Welsher, K.; Tabakman, S. M.; Sherlock, S. P.; Wang, H.; Luong, R.; Dai, H. High Performance in Vivo Near-IR (>1 Mm) Imaging and Photothermal Cancer Therapy with Carbon Nanotubes. *Nano Res.* **2010**, *3* (11), 779−793.

(14) Betzer, O.; Ankri, R.; Motiei, M.; Popovtzer, R. Theranostic Approach for Cancer Treatment: Multifunctional Gold Nanorods for Optical Imaging and Photothermal Therapy. *J. Nanomater.* **2015**, *2015*, 1−7.

(15) Ankri, R.; Fixler, D. Gold Nanorods Based Diffusion Reflection Measurements: Current Status and Perspectives for Clinical Applications. *Nanophotonics* **2017**, *6* (5), 1031−1042.

(16) Dreifuss, T.; Betzer, O.; Shilo, M.; Popovtzer, A.; Motiei, M.; Popovtzer, R. A Challenge for Theranostics: Is the Optimal Particle for Therapy Also Optimal for Diagnostics? *Nanoscale* **2015**, *7* (37), 15175−15184.

(17) Dreifuss, T.; Davidi, E. S.; Motiei, M.; Barnoy, E.; Bragilovski, D.; Lubimov, L.; Kindler, M. J. J.; Popovtzer, A.; Popovtzer, R. All-in-One Theranostic Nanoagent for Head and Neck Cancer Treatment. *Proceedings SPIE 10506, Nanoscale Imaging, Sensing, and Actuation for Biomedical Applicatons XV*; SPIE: Bellingham, WA, USA, 2018; Vol. 10506, DOI: 10.1117/12.2289459.

(18) Reuveni, T.; Motiei, M.; Romman, Z.; Popovtzer, A.; Popovtzer, R. Targeted Gold Nanoparticles Enable Molecular CT Imaging of Cancer: An in Vivo Study. *Int. J. Nanomed.* **2011**, *6*, 2859−2864.

(19) Motiei, M.; Dreifuss, T.; Betzer, O.; Panet, H.; Popovtzer, A.; Santana, J.; Abourbeh, G.; Mishani, E.; Popovtzer, R. Differentiating Between Cancer and Inflammation: A Metabolic-Based Method for Functional Computed Tomography Imaging. *ACS Nano* **2016**, *10* (3), 3469−3477.

(20) Barnoy, E. A. E. A.; Fixler, D.; Popovtzer, R.; Nayhoz, T.; Ray, K. An Ultra-Sensitive Dual-Mode Imaging System Using Metal-Enhanced Fluorescence in Solid Phantoms. *Nano Res.* **2015**, *8* (12), 3912−3921.

(21) Nayhoz, T.; Barnoy, E. A.; Fixler, D. Tissue-like Phantoms as a Platform for Inserted Fluorescence Nano-Probes. *Materials* **2016**, *9* (11), 926.

(22) Fixler, D.; Nayhoz, T.; Ray, K. Diffusion Reflection and Fluorescence Lifetime Imaging Microscopy Study of Fluorophore-Conjugated Gold Nanoparticles or Nanorods in Solid Phantoms. *ACS Photonics* **2014**, *1* (9), 900−905.

(23) Lakowicz, J. R. *Principles of Fluorescence Spectroscopy*, 3rd ed.; Springer: New York, NY, USA, 2006.

(24) Becker, W. Fluorescence Lifetime Imaging–Techniques and Applications. *J. Microsc.* **2012**, *247* (2), 119−136.

(25) Schwartz, S.; Fixler, D.; Popovtzer, R.; Shefi, O. Fluorescence Life-Time Imaging and Steady State Polarization for Examining Binding of Fluorophores to Gold Nanoparticles. *J. Biophotonics* **2015**, *8* (11−12), 944−951.

(26) Ray, K.; Szmacinski, H.; Enderlein, J.; Lakowicz, J. R. Distance Dependence of Surface Plasmon-Coupled Emission Observed Using Langmuir-Blodgett Films. *Appl. Phys. Lett.* **2007**, *90* (25), 251116.

(27) Ray, K.; Badugu, R.; Lakowicz, J. R. Polyelectrolyte Layer-by-Layer Assembly to Control the Distance between Fluorophores and Plasmonic Nanostructures. *Chem. Mater.* **2007**, *19* (24), 5902−5909.

(28) Ray, K.; Zhang, J.; Lakowicz, J. R. Fluorescence Lifetime Correlation Spectroscopic Study of Fluorophore-Labeled Silver Nanoparticles. *Anal. Chem.* **2008**, *80* (19), 7313−7318.

(29) Chandran, H.; Gopalkrishnan, N.; Garg, S.; Reif, J. In *Biomolecular Computing Systems: From Logic Systems to Smart Sensors and Actuators*; Katz, E., Ed.; Wiley-VCH: Weinheim, Germany, 2012.

(30) Miyamoto, T.; Razavi, S.; DeRose, R.; Inoue, T. Synthesizing Biomolecule-Based Boolean Logic Gates. *ACS Synth. Biol.* **2013**, *2* (2), 72−82.

(31) Andréasson, J.; Pischel, U. Molecules with a Sense of Logic: A Progress Report. *Chem. Soc. Rev.* **2015**, *44* (5), 1053−1069.

(32) Evans, A. C.; Thadani, N. N.; Suh, J. Biocomputing Nanoplatforms as Therapeutics and Diagnostics. *J. Controlled Release* **2016**, *240*, 387−393.

(33) Katz, E.; Wang, J.; Halamek, J.; Halamkova, L. Enzyme Logic Systems: Biomedical and Forensic Biosensor Applications. In *Label-Free Biosensing*; Schöning, M., Poghossian, A., Eds.; Springer: Cham, Switzerland, 2017; Vol. 16, pp 345−381, DOI: 10.1007/5346_2017_4.

(34) Nikitin, M. P.; Shipunova, V. O.; Deyev, S. M.; Nikitin, P. I. Biocomputing Based on Particle Disassembly. *Nat. Nanotechnol.* **2014**, *9*, 716−722.

(35) Angelos, S.; Yang, Y.; Khashab, N. M.; Stoddart, J. F.; Zink, J. I. Dual-Controlled Nanoparticles Exhibiting AND Logic. *J. Am. Chem. Soc.* **2009**, *131*, 11344−11346.

(36) Han, H.; Valdepérez, D.; Jin, Q.; Yang, B.; Li, Z.; Wu, Y.; Pelaz, B.; Parak, W. J.; Ji, J. Dual Enzymatic Reaction-Assisted Gemcitabine Delivery Systems for Programmed Pancreatic Cancer Therapy. *ACS Nano* **2017**, *11* (2), 1281−1291.

(37) Yan, C.; Guo, Z.; Liu, Y.; Shi, P.; Tian, H.; Zhu, W. H. A Sequence-Activated and Logic Dual-Channel Fluorescent Probe for Tracking Programmable Drug Release. *Chem. Sci.* **2018**, *9* (29), 6176−6182.

(38) Razgulin, A.; Ma, N.; Rao, J. Strategies for in Vivo Imaging of Enzyme Activity: An Overview and Recent Advances. *Chem. Soc. Rev.* **2011**, *40* (7), 4186−4216.

(39) Hutter, E.; Maysinger, D. Gold-Nanoparticle-Based Biosensors for Detection of Enzyme Activity. *Trends Pharmacol. Sci.* **2013**, *34* (9), 497−507.

(40) Zhang, J.; Li, C.; Zhang, X.; Huo, S.; Jin, S.; An, F.-F.; Wang, X.; Xue, X.; Okeke, C. I.; Duan, G.; Guo, F.; Zhang, X.; Hao, J.; Wang, P. C.; Zhang, J.; Liang, X.-J. In Vivo Tumor-Targeted Dual-Modal Fluorescence/CT Imaging Using a Nanoprobe Co-Loaded with an Aggregation-Induced Emission Dye and Gold Nanoparticles. *Biomaterials* **2015**, *42*, 103−111.

(41) Drake, C. R.; Miller, D. C.; Jones, E. F. Activatable Optical Probes for the Detection of Enzymes. *Curr. Org. Synth.* **2011**, *8* (4), 498−520.

(42) Cheng, W.; Chen, Y.; Yan, F.; Ding, L.; Ding, S.; Ju, H.; Yin, Y. Ultrasensitive Scanometric Strategy for Detection of Matrix Metalloproteinases Using a Histidine Tagged Peptide-Au Nanoparticle Probe. *Chem. Commun. (Cambridge, U. K.)* **2011**, *47* (10), 2877−2879.

(43) Park, S. Y.; Lee, S. M.; Kim, G. B.; Kim, Y.-P. Gold Nanoparticle-Based Fluorescence Quenching via Metal Coordination for Assaying Protease Activity. *Gold Bull.* **2012**, *45*, 213−219.

(44) Tira, D. S.; Focsan, M.; Ulinici, S.; Maniu, D.; Astilean, S. Rhodamine B-Coated Gold Nanoparticles as Effective "Turn-on" Fluorescent Sensors for Detection of Zinc II Ions in Water. *Spectrosc. Lett.* **2014**, *47* (2), 153−159.

(45) Geddes, C.; Lakowicz, J. Metal-Enhanced Fluorescence. *J. Fluoresc.* **2002**, *12* (2), 121−129.

(46) Abadeer, N.; Brennan, M.; Wilson, W.; Murphy, C. Distance and Plasmon Wavelength Dependent Fluorescence of Molecules Bound to Silica-Coated Gold Nanorods. *ACS Nano* **2014**, *8* (8), 8392−8406.

(47) Kang, K.a; Wang, J. Smart Dual-Mode Fluorescent Gold Nanoparticle Agents. *Wiley Interdiscip. Rev. Nanomed. Nanobiotechnol.* **2014**, *6* (4), 398−409.

(48) Mahajan, P. G.; Kolekar, G. B.; Patil, S. R. Fluorescence-Based Logic Gate for Sensing of Ca²⁺ and F⁻ Ions Using PVP Crowned Chrysene Nanoparticles in Aqueous Medium. *Luminescence* **2017**, *32* (5), 845−854.

(49) Liao, S.; Li, X.; Yang, H.; Chen, X. Nitrogen-Doped Carbon Dots Rapid and Selective Detection of Mercury Ion and Biothiol and Construction of an IMPLICATION Logic Gate. *Talanta* **2019**, *194*, 554−562.

(50) Zou, W.-S.; Zhao, Q.-C.; Kong, W.-L.; Wang, X.-F.; Chen, X.-M.; Zhang, J.; Wang, Y.-Q. Multi-Level Fluorescent Logic Gate Based on Polyamine Coated Carbon Dots Capable of Responding to Four Stimuli. *Chem. Eng. J.* **2018**, *337*, 471−479.

(51) Remón, P.; Ferreira, R.; Montenegro, J.-M.; Suau, R.; Pérez-Inestrosa, E.; Pischel, U. Reversible Molecular Logic: A Photophysical Example of a Feynman Gate. *ChemPhysChem* **2009**, *10* (12), 2004−2007.

(52) Yuan, Y.; Jiang, J.; Liu, S.; Yang, J.; Zhang, H.; Yan, J.; Hu, X. Fluorescent Carbon Dots for Glyphosate Determination Based on Fluorescence Resonance Energy Transfer and Logic Gate Operation. *Sens. Actuators, B* **2017**, *242*, 545−553.

(53) Wiesel-Kapah, I.; Kaminka, G. A.; Hachmon, G.; Agmon, N.; Bachelet, I. Rule-Based Programming of Molecular Robot Swarms for Biomedical Applications. *Proceedings of the Twenty-Fifth International Joint Conference on Aritficial Intelligence (IJCAI-16)*; pp 3505−3512.

(54) Barnoy, E. A.; Popovtzer, R.; Fixler, D. Implementing Biological Logic Gates Using Gold Nanoparticles Conjugated to Fluorophores. *Proceedings of SPIE 10506, Nanoscale Imaging, Sensing, and Actuation for Biomedical Applications XV*; SPIE: Bellingham, WA, USA, 2018; Vol. *10506*, DOI: 10.1117/12.2287097.

(55) Barnoy, E. A.; Popovtzer, R.; Fixler, D. Development of a Molecular Bioswitch Using Fluorescence Lifetime Imaging: Incremental Activation of Fluorescein Diacetate. *J. Biophotonics* **2018**, *11* (2), No. e201700084.

(56) Rick, W. Trypsin. In *Methods of Enzymatic Analysis*, 2nd ed.; Bergmeyer, H. U., Ed.; Academic Press: New York, NY, USA, 1974; pp 1013−1024.

(57) Enüstün, B. V.; Turkevich, J. Coagulation of Colloidal Gold. *J. Am. Chem. Soc.* **1963**, *85* (21), 3317−3328.

(58) Fluorescein, Oregon Green and Rhodamine Green Dyes. In *Molecular Probes Handbook: A Guide to Fluorescent Probes and Labeling Technologies*; Johnson, I., Spence, M., Eds.; Life Technologies, 2010; pp 66−73.

(59) Rusinova, E.; Tretyachenko-Ladokhina, V.; Vele, O. E.; Senear, D. F.; Alexander Ross, J. B. Alexa and Oregon Green Dyes as Fluorescence Anisotropy Probes for Measuring Protein-protein and Protein-nucleic Acid Interactions. *Anal. Biochem.* **2002**, *308* (1), 18−25.

(60) Bovey, F. A.; Yanari, S. S. *The Enzymes*, Vol. 4, 2nd ed.;Boyer, P. D., Lardy, H., Myrback, K., Eds.; Academic Press: New York, NY, USA, 1960.

(61) Samuels, T. L.; Johnston, N. Pepsin as a Marker of Extraesophageal Reflux. *Ann. Otol., Rhinol., Laryngol.* **2010**, *119* (3), 203−208.

(62) Bardhan, K. D.; Strugala, V.; Dettmar, P. W. Reflux Revisited: Advancing the Role of Pepsin. *Int. J. Otolaryngol.* **2012**, *2012*, 646901.

(63) Jang, B.; Choi, Y. Photosensitizer-Conjugated Gold Nanorods for Enzyme-Activatable Fluorescence Imaging and Photodynamic Therapy. *Theranostics* **2012**, *2* (2), 190−197.

(64) Eckhard, U.; Huesgen, P. F.; Schilling, O.; Bellac, C. L.; Butler, G. S.; Cox, J. H.; Dufour, A.; Goebeler, V.; Kappelhoff, R.; Keller, U. D.; Klein, T.; Lange, P. F.; Marino, G.; Morrison, C. J.; Prudova, A.; Rodriguez, D.; Starr, A. E.; Wang, Y.; Overall, C. M. Active Site Specificity Profiling of the Matrix Metalloproteinase Family: Proteomic Identification of 4300 Cleavage Sites by Nine MMPs Explored with Structural and Synthetic Peptide Cleavage Analyses. *Matrix Biol.* **2016**, *49*, 37−60.

(65) Ankri, R.; Leshem-Lev, D.; Fixler, D.; Popovtzer, R.; Motiei, M.; Kornowski, R.; Hochhauser, E.; Lev, E. I. Gold Nanorods as Absorption Contrast Agents for the Noninvasive Detection of Arterial Vascular Disorders Based on Diffusion Reflection Measurements. *Nano Lett.* **2014**, *14* (5), 2681−2687.

(66) Kang, K.; Wang, J. Conditionally Activating Optical Contrast Agent with Enhanced Sensitivity via Gold Nanoparticle Plasmon Energy Transfer: Feasibility Study. *J. Nanobiotechnol.* **2014**, *12* (1), 56.

(67) Hu, Z.; Ma, J.; Fu, F.; Cui, C.; Li, X.; Wang, X.; Wang, W.; Wan, Y.; Yuan, Z. An Intelligent Re-Shieldable Targeting System for Enhanced Tumor Accumulation. *J. Controlled Release* **2017**, *268*, 1−9.

(68) Zhao, X.; Yang, C. X.; Chen, L. G.; Yan, X. P. Dual-Stimuli Responsive and Reversibly Activatable Theranostic Nanoprobe for Precision Tumor-Targeting and Fluorescence-Guided Photothermal Therapy. *Nat. Commun.* **2017**, *8*, 14998.

(69) Amir, Y.; Ben-Ishay, E.; Levner, D.; Ittah, S.; Abu-Horowitz, A.; Bachelet, I. Universal Computing by DNA Origami Robots in a Living Animal. *Nat. Nanotechnol.* **2014**, *9* (5), 353−357.

(70) Kaminka, G. A.; Spokoini-Stern, R.; Amir, Y.; Agmon, N.; Bachelet, I. Molecular Robots Obeying Asimov's Three Laws of Robotics. *Artif. Life* **2017**, *23* (3), 343−350.